IEEE Access
Multidisciplinary : Rapid Review : Open Access Journal

Received 18 November 2023, accepted 4 December 2023, date of publication 12 December 2023,
date of current version 21 December 2023.

Digital Object Identifier 10.1109/ACCESS.2023.3341867

RESEARCH ARTICLE

Calculation Model of Parasitic Capacitance for High-Frequency Inductors and Transformers

YUJIE LAN[1], LEI YANG[2], XU ZHANG[1], QINGBIN CHEN[1], AND ZAIPING ZHENG[2]
[1]School of Electrical Engineering and Automation, Fuzhou University, Fuzhou 350108, China
[2]Beijing Institute of Precision Mechatronics and Controls, Beijing 100076, China

Corresponding author: Qingbin Chen (cqb@fzu.edu.cn)

ABSTRACT With high power density and high-frequency power electronics technologies, parasitic capacitances of inductors and transformers have been widely discussed, in which parasitic capacitance may lead to electromagnetic interference (EMI) and efficiency performance degradation. Therefore, it is significant to analyze and model the parasitic capacitance of the inductors and transformers. This paper proposes a new parasitic capacitance calculated model of multilayer windings inductors and transformers. Based on the electromagnetic field theory, it can fully consider the edge effect of multilayer inductor windings, including the edge effect between adjacent and non-adjacent layers. Finally, the accuracy of the model is validated by simulation and experiment. Compared with the traditional parasitic capacitance calculated method, the proposed model can calculate the parasitic capacitance more accurately, and the maximum error between calculations and simulations is less than 8%.

INDEX TERMS Parasitic capacitance, edge effect, modeling, inductor.

I. INTRODUCTION

With the development of high-frequency power electronics technology, especially wide band gap semiconductors such as SiC and GaN, the magnetic components, including high-frequency inductors and transformers, have become a hot research topic in recent years [1]. As the switching frequency increases, the influence of the parasitic parameters of magnetic components becomes increasingly important, especially parasitic capacitance, which may result in electromagnetic interference (EMI) and efficiency degradation [2].

In high-frequency applications, the parasitic capacitance may oscillate with the inductance of the magnetic components, worsen the electromagnetic environment, and increase unnecessary losses. Moreover, the high voltage stress generated by oscillation may destroy the magnetic components' insulation, threaten the system's reliability, and affect the equipment's normal operation [3], [4], [5]. Therefore, to achieve an optimized magnetic component design, it is very important to analyze the influencing factors of distributed capacitance and theoretically calculate the parasitic capacitance value.

The associate editor coordinating the review of this manuscript and approving it for publication was Giambattista Gruosso.

In [6] and [7], the parasitic parameters of transformers were analyzed by combining the Finite Element Method (FEM), considering different magnetic cores and winding structures. Ultimately, a transformer design method considering parasitic parameters was proposed, but simulation modeling is often time-consuming. In [8], the transformer capacitance is extracted through experiments. This method's parasitic capacitance can only be extracted after the transformer is manufactured, which is unsuitable for the parasitic capacitance prediction before it is made and cannot be optimized in the design process.

In [9] and [10], these methods are based on the static capacitance of turn-turn and layer-layer winding. However, when the interlayer spacing in multilayer windings is small compared to the winding height, these methods do not account for edge effects.

In [11] and [12], a method is proposed to calculate the inter-turn capacitance by simulating the electric field lines between adjacent coils, but this method was only applicable to circular straight wires and could not calculate the inter-turn capacitance of non-adjacent turns. Moreover, magnetic components' windings are equivalent to cylindrical or plate capacitors in many papers [13], [14], [15], [16], [17]. However, these studies do not consider the electrical field around the edges of winding layers (called edge effects in this paper). The equivalent capacitance of the electric field energy W_{ll} due to edge effects is represented by C_{edge} in Fig. 1. In the winding interior, the electric field distribution is similar to cylindrical or plate capacitors. However, at the edges of the winding layers, the electric field distribution becomes quite different due to the influence of the winding's geometry and the surrounding environment. Now, research on the edge effects of inductors mainly focuses on the losses of the winding turns, while studies on the electric field energy are still scarce [18], [19], [20]. When the interlayer spacing is not small enough compared to the winding height, such as planar magnetic components with wire wound winding, the energy concentrated in the edge regions cannot be neglected.. Neglecting the electric field intensity in this region can lead to significant computational errors. In [17], the edge effects parasitic capacitance is discussed, and a coefficient obtained by FEA simulation is used to calculate the edge effects parasitic capacitance. However, this coefficient may not be suitable for all structures and sizes.

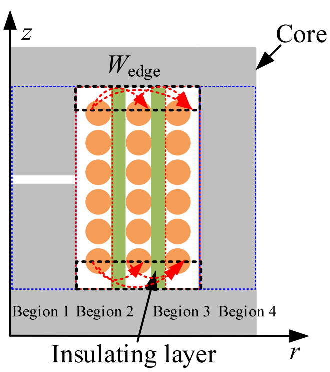

FIGURE 1. The 2D model of the inductor.

This paper proposes a novel method for calculating the parasitic capacitance of multilayer magnetic components. The approach involves computing the end-field energy at the edges of multiple layers of inductors, optimizing the conventional practice of equivalent representation of windings as cylindrical or parallel-plate capacitors. Through simulation and experimentation, it has been demonstrated that this method accurately calculates the parasitic capacitance of inductor.

The rest of this paper is organized as follows. Section II analyzes three parts of parasitic capacitors in high-frequency inductors, and the normal energy proportion of different parts is presented. Section III analyzes the traditional capacitance calculation method, which ignores the influence of the edge effect. It is unsuitable for the parasitic capacitance calculation of planar magnetic components with wire wound winding. Section IV proposes a new parasitic capacitance method, which considers the edge effects. Section V makes a high-frequency inductor and compares the parasitic capacitance of the simulation, measured and calculated results.

II. DISTRIBUTED CAPACITANCE MODEL OF HIGH FREQUENCY INDUCTOR

The 2D model of the high-frequency inductor in the *r-z* coordinate system is shown in Fig. 1.

There are three parts of capacitances in the inductor, which are inter-turn capacitance C_{tt} in *Fig. 2(a)*, interlayer capacitance C_{ll} in Fig. 2(b) and layer-to-core capacitance C_{lc} in Fig. 2(c).

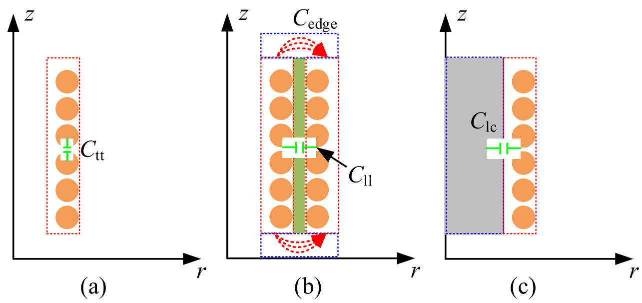

FIGURE 2. The 2D model of three parts capacitance in the inductor.

The total equivalent parasitic capacitance C_D can be calculated by equation (1) based on the energy method.

$$\begin{cases} W = \frac{1}{2} \cdot C_D \cdot U^2 \\ W = W_{tt} + W_{ll} + W_{lc} \end{cases} \tag{1}$$

where U is the inductor's voltage, W_{tt}, W_{ll} and W_{lc} are the energy generated by inter-turns, interlayers, and winding-to-core capacitance. W_{edge} refers to the end energy and is included in W_{ll}.

In order to obtain the proportion of the three kinds of energy, a simulation of the 3-layer, 15-turn inductor is built, whose model is shown in Fig. 1, and simulated in ANSYS electromagnetic simulation software. The simulation results show the energy proportion in Fig.3. Among them, W_{edge} is the energy at the end, which is included in W_{ll}. The W_{tt} is much smaller than the other parts. This is because, in multilayer windings, which often have many turns, the capacitance between inter-turns is relatively small and can be ignored [13], [14]. Therefore, only the interlayer and winding-to-core capacitance are considered when calculating the equivalent parasitic capacitance of inductors. In comparison, the traditional calculation method is equivalent to a cylindrical capacitor.

A. THE TRADITIONAL CALCULATION MODEL OF THE PARASITIC CAPACITANCE

The 2D model of a two-layer winding is shown in Fig. 4. The interlayer capacitance and winding-to-core capacitance can be equivalent to a cylindrical capacitor.

Assuming that the potential of cylindrical capacitor linearly increases from U_{AO} to U_{AD}, and the potential of cylindrical B linearly increases from U_{BO} to U_{BD}. b_w is the layer's height, ε_r is the relative permittivity of the insulating layer.

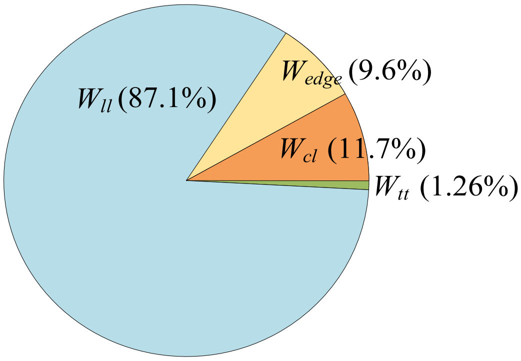

FIGURE 3. Energy ratio of three parts capacitance in the inductor.

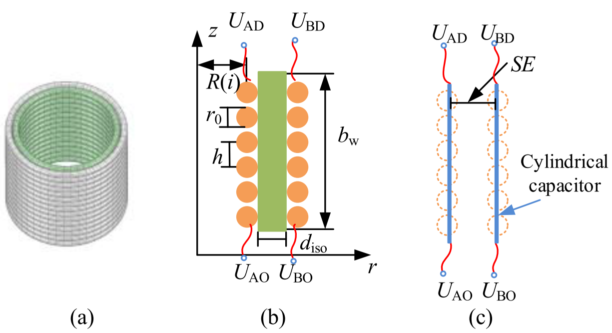

FIGURE 4. The inter-layer and winding to core capacitance analysis. (a) is a 3D schematic diagram of the two-layer winding, (b) is a 2D schematic diagram of the two-layer winding, and (c) is a cylindrical capacitor model diagram representing the equivalent winding.

The interlayer energy W_{ll} can be calculated by equation (2):

$$\begin{cases} W_{ll} = \dfrac{C_{ll}}{6} \cdot (U_O^2 + U_O \cdot U_D + U_D^2) \\ C_{ll} = \dfrac{2 \cdot \pi \varepsilon_0 \varepsilon_r b_w}{\ln(\frac{R+SE}{R})} \\ U_O = U_{BO} - U_{AO}, U_D = U_{BD} - U_{AD} \\ R = R(i) + \dfrac{r_0 + d_{iso} - SE}{2} \\ SE = d_{iso} - 1.15 r_0 + 0.26 h \end{cases} \tag{2}$$

The layer-to-core energy W_{ll} can be calculated by (3):

$$\begin{cases} C_{lc} = \dfrac{2 \cdot \pi \varepsilon_0 \varepsilon_r b_{wlc}}{\ln(\frac{R_{lc}+SC1}{R_{lc}})} \\ R = R_1(i) + \dfrac{d_{core} - SC}{2} \\ U_{O1} = U_{BO1} - U_{AO1}, U_{D1} = U_{BD1} - U_{AD1} \\ W_{lc} = \dfrac{C_{lc}}{6} \cdot (U_O^2 + U_O \cdot U_D + U_D^2) \\ SC1 = d_{core1} + \dfrac{1}{2} \cdot (0.26 h_{lc} - 1.15 r_{0lc}) \end{cases} \tag{3}$$

B. ANALYSIS OF EDGE EFFECT

The electrical field distribution of the edge portion of the inductor and its surrounding environment differ from those within the interior portion. The traditional equivalent calculation method of cylindrical or plate capacitors only considers the electric field between cylindrical (W_A) and does not consider the distribution of the electric field in the edge ($W_B + W_C$), as shown in Fig. 5.

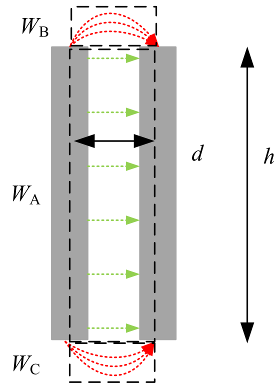

FIGURE 5. The electric field distribution of cylindrical capacitor.

Combined with the finite element simulation software (FEA), a specific plate capacitor is taken as an example to analyze the influence of the edge effect. Under different ratios of interlayer distance d and height h, the ratio of electric field energy ($W_B + W_C$) generated by the edge to the total energy ($W_A + W_B + W_C$) of the capacitor changes, as shown in Fig. 6(a). Moreover, the calculation error of electrical filed energy of plate capacitor in different d/h is shown in Fig. 6(b).

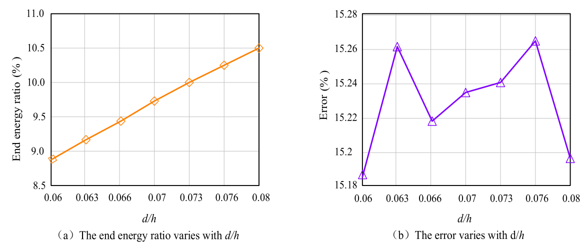

FIGURE 6. Interlayer energies of different d and h.

As seen from Fig. 6, with the increase of d/h, the energy stored in the edge of the plate capacitor keeps increasing. Moreover, the calculation error is larger than 15%.

Fig. 6 illustrates that when the interlayer spacing of the inductor is relatively big compared to its overall height, the electric or magnetic fields at the edge portion may spread to a wide space, resulting in edge effects. Therefore, it is necessary to consider the influence of the electric field at the edge when calculating the interlayer capacitance of the inductor.

III. CAPACITANCE CALCULATION METHOD CONSIDERING EDGE EFFECTS

According to the above analysis, the edge effect cannot be ignored when d/h is large. Therefore, a method for calculating the edge effect energy is proposed in this paper.

For inductors wound with circular wires, the interlayer edge effect can be equivalent to a concentric circle structure, and its 2D equivalent model is shown in Fig. 7. Taking the winding turns i and j as examples, the calculation method of layer-to-layer edge capacitance is analyzed.

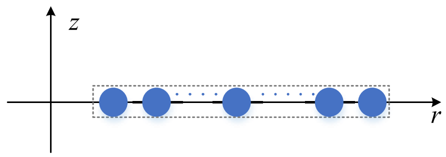

FIGURE 7. Interlayer edge effect equivalent model of a 2D inductor.

Fig.8(b) is a top view of Fig.8(a), establishing a polar coordinate system to describe the winding edge of Figure 8(a). Charge Q and -Q are attached to parallel plate capacitors i and j, respectively. In the polar coordinate system, if the distance between two wires is much larger than the wire diameter, that is, when (r_j-r_i) is much larger than the wire diameter, the influence of the wire diameter of the coil can be ignored. Then, the electric field intensity is caused by the charge element dq (Since the charge is concentrated on the electrical axis, it is assumed that the charge is uniformly distributed on the electrical axis. When a segment of the electrical axis that is infinitesimally small is taken, the amount of charge on that segment is the charge element) on winding turn i at some point P in space can be calculated by the formula (4):

$$\begin{cases} d\vec{E}_{\mathrm{ri}} = dE_{\mathrm{i}} \cos(\alpha) \vec{e}_{\mathrm{r}} \\ \cos(\alpha) = \dfrac{r_0^2 + r^2 - r_{\mathrm{i}}^2}{2 r_0 r} \\ \vec{E}_{\mathrm{ri}} = \displaystyle\int_0^{2\pi} d\vec{E}_{\mathrm{ri}} \end{cases} \tag{4}$$

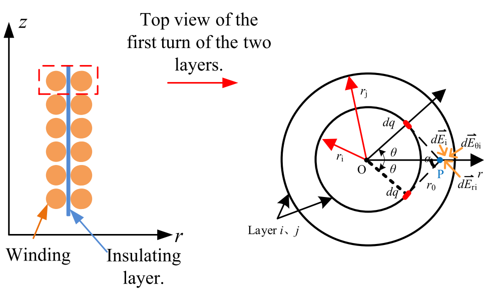

FIGURE 8. Top view between two layers.

Since the distance between the layers is small, the distance between i and j is small at this time, and the wire diameter of the coil will not be ignored compared to the wire diameter. Due to the influence of wire diameter and distance, the position of its electrical axis has changed and is no longer the center position of the coil. In this paper, the electric axis theory is adopted. Its electrical axis position is shown in Figure 9; according to the electric axis theory, the electrical axis position can be calculated by (5):

$$\begin{cases} a_0 = \sqrt{(\dfrac{r_{\mathrm{j}} - r_{\mathrm{i}}}{2})^2 - (\dfrac{d}{2})^2} \\ \Delta = \dfrac{r_{\mathrm{j}} - r_{\mathrm{i}}}{2} - a_0 \end{cases} \tag{5}$$

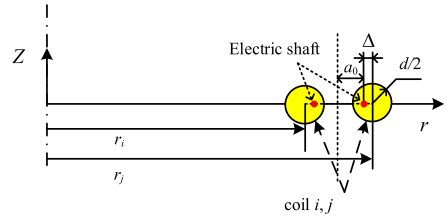

FIGURE 9. Consider the shaft position of the coil conductor diameter.

According to the symmetry of winding turns i and j, the electric field strength dE_i component of the charge Q carried by layer i at point P is canceled out with each other, and only the component dE_{ri} in the r direction exists. Similarly, the electric field strength of the charge -Q on the j at point P is dE_{rj}. For this reason, by using the field strength superposition theorem, the total electric field strength at point P in space is shown in (6):

$$\begin{aligned} \vec{E}_{\mathrm{r}} &= \vec{E}_{\mathrm{ri}} + \vec{E}_{\mathrm{rj}} \\ &= \int_0^{2\pi} \frac{Q[r - (r_{\mathrm{i}} + \Delta)\cos(\theta)]}{8\pi^2 \varepsilon_0 [(r_{\mathrm{i}} + \Delta)^2 + r^2 - 2(r_{\mathrm{i}} + \Delta) r \cos(\theta)]^{1.5}} d\theta \\ &\quad + \int_0^{2\pi} \frac{-Q[r - (r_{\mathrm{j}} - \Delta)\cos(\theta)]}{8\pi^2 \varepsilon_0 [(r_{\mathrm{j}} - \Delta)^2 + r^2 - 2(r_{\mathrm{j}} - \Delta) r \cos(\theta)]^{1.5}} d\theta \end{aligned} \tag{6}$$

where ε_0 is the vacuum permittivity.

Then, the capacitance C_{ij} of winding turns i and j can be obtained by equation (7):

$$\begin{cases} U_{\mathrm{ij}} = \int_{r_{\mathrm{i}}+d/2}^{r_{\mathrm{j}}-d/2} \vec{E}_{\mathrm{r}} dr \\ C_{\mathrm{ij}} = \frac{Q}{U_{\mathrm{ij}}} \end{cases} \tag{7}$$

Combining the (4), (6) and (7), C_{ij} can be simplified to:

$$\begin{aligned} C_i = \Bigg\{ &\int_{\mathrm{i}+\Delta/2}^{r-\alpha iz} \\ &\times \Bigg(\int_0^{\pi} \frac{[\mathrm{r} - (\mathrm{r} + \Delta)\cos(\theta)]}{8\pi^2 \varepsilon_0 \left[(\mathrm{r}+\Delta)^2 + \mathrm{r}^2 - 2(\mathrm{r}+\Delta)\mathrm{r}\cos(\theta)\right]^{13}} \mathrm{d}\theta \\ &+ \int_0^{2\pi} \frac{-[r - (r_i - \Delta)\cos(\theta)]}{8\pi^2 \varepsilon_0 \left[(r_i - \Delta)^2 + r^2 - 2(r - \Delta) r \cos(\theta)\right]^{15}} d\theta \Bigg) dr \Bigg\}^{-1} \end{aligned} \tag{8}$$

According to the equation (8), The edge capacitance between the two layers of windings can be obtained. However, if the number of layers exceeds 2, the potential at any point P will no longer be determined by two charge elements dq, and therefore, the above equation will no longer be applicable. Then, take a three-layer winding as an example to solve the edge capacitance. Its 2D model is shown in Fig. 10. It represents a top view of the uppermost loop of a three-layer inductor winding.

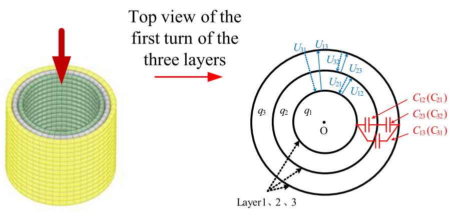

FIGURE 10. Schematic diagram of the structure of the three layers.

The charge of each turn coil is q_1, q_2 and q_3, respectively. Moreover, the layer-to-layer edge voltage is U_{12}, U_{23} and U_{13}, respectively. The edge capacitance is C_{12}, C_{23} and C_{13}, respectively. Then:

$$\begin{cases} q_1 = C_{12}U_{12} + C_{13}U_{13} \\ q_2 = C_{21}U_{21} + C_{23}U_{23} \\ q_3 = C_{31}U_{31} + C_{32}U_{32} \end{cases} \tag{9}$$

where $C_{12} = C_{21}$, $C_{23} = C_{32}$, $C_{13} = C_{31}$ and U_{12} = -U_{21}, U_{23} = -U_{32}, U_{13} = -U_{31}.

The edge effect capacitance is only related to the winding structure. Different charges of q_1, q_2 and q_3 only affect the voltage of winding turns, so this paper proposes to solve the winding turns' voltage under different charge setups. Finally, it can get the edge effects capacitance of the layers. A three-layer winding needs at least two matrixes of charge distributions to solve the edge capacitance.

Assuming that the two matrixes of charge distributions are $[q]_{<1>}$ and $[q]_{<2>}$, as shown in (10):

$$\begin{cases} [q]_{<1>} = [q_1 q_2 q_3] = [Q - Q0] \\ [q]_{<2>} = [q_1 q_2 q_3] = [0Q - Q] \end{cases} \tag{10}$$

When the charge distribution is $[q]_{<1>}$, the voltage of different turns can be expressed by (11):

$$\begin{cases} U_{12<1>} = \displaystyle\int_{r_0/2}^{h-r_0/2} \left[\begin{array}{l} \int_0^{2\pi} \frac{Q\cdot(h_0-\Delta)}{8\pi^2\varepsilon_0[R(i)^2+R(i)^2-2R(i)\cdot R(i)\cos(\theta)+(h_0-\Delta)^2]^{1.5}}d\theta \\ +\int_0^{2\pi} \frac{Q\cdot(h-h_0-\Delta)}{8\pi^2\varepsilon_0[R(i)^2+R(i)^2-2R(i)\cdot R(i)\cos(\theta)+(h-h_0-\Delta)^2]^{1.5}}d\theta \end{array}\right] dh_0 \\ U_{23<1>} = \displaystyle\int_{h+r_0/2}^{2h-r_0/2} \left[\begin{array}{l} \int_0^{2\pi} \frac{Q\cdot h_0}{8\pi^2\varepsilon_0[R(i)^2+R(i)^2-2R(i)\cdot R(i)\cos(\theta)+(h_0)^2]^{1.5}}d\theta \\ +\int_0^{2\pi} \frac{Q\cdot(h-h_0)}{8\pi^2\varepsilon_0[R(i)^2+R(i)^2-2R(i)\cdot R(i)\cos(\theta)+(h-h_0)^2]^{1.5}}d\theta \end{array}\right] dh_0 \\ U_{13<1>} = U_{12<1>} + U_{23<1>} \end{cases} \tag{11}$$

According to equations (9) and (11), then:

$$\begin{cases} Q = C_{12}\cdot U_{12<1>} + C_{13}\cdot U_{13<1>} \\ -Q = C_{21}\cdot(-U_{12<1>}) + C_{23}\cdot U_{23<1>} \\ 0 = C_{31}\cdot(-U_{13<1>}) + C_{32}\cdot(-U_{23<1>}) \end{cases} \tag{12}$$

Similarly, for the charge distribution $[q]_{<2>}$, the voltage of different turns can be got:

$$\begin{cases} U_{12<2>} = \displaystyle\int_{r_0/2}^{h-r_0/2} \left[\begin{array}{l} \int_0^{2\pi} \frac{Q\cdot(h_0-h)}{8\pi^2\varepsilon_0[R(i)^2+R(i)^2-2R(i)\cdot R(i)\cos(\theta)+(h-h_0)^2]^{1.5}}d\theta \\ +\int_0^{2\pi} \frac{Q\cdot(2h-h_0)}{8\pi^2\varepsilon_0[R(i)^2+R(i)^2-2R(i)\cdot R(i)\cos(\theta)+(2h-h_0)^2]^{1.5}}d\theta \end{array}\right] dh_0 \\ U_{23<2>} = \displaystyle\int_{h+r_0/2}^{2h-r_0/2} \left[\begin{array}{l} \int_0^{2\pi} \frac{Q\cdot(h_0-h-\Delta)}{8\pi^2\varepsilon_0[R(i)^2+R(i)^2-2R(i)\cdot R(i)\cos(\theta)+(h_0-h-\Delta)^2]^{1.5}}d\theta \\ +\int_0^{2\pi} \frac{Q\cdot(2h-h_0-\Delta)}{8\pi^2\varepsilon_0[R(i)^2+R(i)^2-2R(i)\cdot R(i)\cos(\theta)+(2h-h_0-\Delta)^2]^{1.5}}d\theta \end{array}\right] dh_0 \\ U_{13<2>} = U_{12<2>} + U_{23<2>} \end{cases} \tag{13}$$

$$\begin{cases} 0 = C_{12}\cdot U_{12<2>} + C_{13}\cdot U_{13<2>} \\ Q = C_{21}\cdot(-U_{12<2>}) + C_{23}\cdot U_{23<2>} \\ -Q = C_{31}\cdot(-U_{13<2>}) + C_{32}\cdot(-U_{23<2>}) \end{cases} \tag{14}$$

According to equations (12) and (14), the edge effect capacitance C_{12}, C_{23}, and C_{13} can be obtained. Moreover, this method can effectively calculate the edge effect capacitance C_{13}.

By this method, the N-turn coil's parasitic capacitance can be obtained. It needs to define (N-1) charge distribution matrixes to solve the N-turn coil's edge effect capacitance. The (N-1) matrixes can be determined according to equation (15), ensuring that each matrix is not repeated.

$$[q]_{<\mathrm{k}>} = \begin{bmatrix} 0 & \ldots & 0 & q_{\mathrm{k}} = Q & q_{\mathrm{k+1}} = -Q & 0 & \ldots & 0 \end{bmatrix} \\ \{k|\ k < N \quad \text{and} \quad k \in N_+\} \tag{15}$$

where $[q]_{<\mathrm{k}>}$ is the k th matrix of charge distributions, q_{k} and $q_{\mathrm{k+1}}$ are the charge of kth turn and k+1th turn, respectively. Then, the adjacent layer voltage can be calculated by equation (16) when charge distributions are $[q]_{<\mathrm{k}>}$.

$$\begin{cases} U_{\mathrm{k(k+1)}} = \displaystyle\int_{(k-1)\cdot h+r_0/2}^{k\cdot h-r_0/2} \left[\begin{array}{l} \int_0^{2\pi} \frac{Q\cdot[h_0-(k-1)h-\Delta]}{8\pi^2\varepsilon_0[R(i)^2+R(i)^2-2R(i)\cdot R(i)\cos(\theta)+[h_0-(k-1)h-\Delta]^2]^{1.5}}d\theta \\ +\int_0^{2\pi} \frac{Q\cdot(kh-h_0-\Delta)}{8\pi^2\varepsilon_0[R(i)^2+R(i)^2-2R(i)\cdot R(i)\cos(\theta)+(kh-h_0-\Delta)^2]^{1.5}}d\theta \end{array}\right] dh_0 \\ \underset{1\le m<N,m\ne k}{U_{\mathrm{m(m+1)}}} = \displaystyle\int_{(m-1)\cdot h+r_0/2}^{m\cdot h-r_0/2} \left[\begin{array}{l} \int_0^{2\pi} \frac{Q\cdot[h_0-(m-1)h]}{8\pi^2\varepsilon_0[R(i)^2+R(i)^2-2R(i)\cdot R(i)\cos(\theta)+[h_0-(m-1)h]^2]^{1.5}}d\theta \\ +\int_0^{2\pi} \frac{Q\cdot(mh-h_0)}{8\pi^2\varepsilon_0[R(i)^2+R(i)^2-2R(i)\cdot R(i)\cos(\theta)+(mh-h_0)^2]^{1.5}}d\theta \end{array}\right] dh_0 \end{cases} \tag{16}$$

According to Kirchhoff's voltage law, the adjacent layer voltage can calculate the voltage between non-adjacent winding turns. Hence, the capacitance between the kth layer winding and other turns can be calculated. Take the first turn of the winding as an example. Its charge matrix can be expressed by equation (17).

$$\begin{bmatrix} q_{1<1>} \\ q_{1<2>} \\ \vdots \\ q_{1<N\text{-}2>} \\ q_{1<N-1>} \end{bmatrix} = \begin{bmatrix} U_{12<1>} & U_{13<1>} & n\ldots & U_{1(N\text{-}1)<1>} & U_{1N<1>} \\ U_{12<2>} & U_{13<2>} & \ldots & U_{1(N\text{-}1)<2>} & U_{1N<2>} \\ \vdots & \vdots & \vdots & \vdots & \vdots \\ U_{12<N\text{-}2>} & U_{13<N\text{-}2>} & \ldots & U_{1(N\text{-}1)<N\text{-}2>} & U_{1N<N\text{-}2>} \\ U_{12<N\text{-}1>} & U_{13<N\text{-}1>} & \ldots & U_{1(N\text{-}1)<N\text{-}1>} & U_{1N<N\text{-}1>} \end{bmatrix} \cdot \begin{bmatrix} C_{12} \\ C_{13} \\ \vdots \\ C_{1(N\text{-}1)} \\ C_{1N} \end{bmatrix} \tag{17}$$

According to equation (17), the edge effect capacitance of the first turn of the winding can be obtained by equation (18).

$$\begin{bmatrix} C_{12} \\ C_{13} \\ \vdots \\ C_{1(N\text{-}1)} \\ C_{1N} \end{bmatrix} = \begin{bmatrix} U_{12<1>} & U_{13<1>} & \ldots & U_{1(N\text{-}1)<1>} & U_{1N<1>} \\ U_{12<2>} & U_{13<2>} & \ldots & U_{1(N\text{-}1)<2>} & U_{1N<2>} \\ \vdots & \vdots & \vdots & \vdots & \vdots \\ U_{12<N\text{-}2>} & U_{13<N\text{-}2>} & \ldots & U_{1(N\text{-}1)<N\text{-}2>} & U_{1N<N\text{-}2>} \\ U_{12<N\text{-}1>} & U_{13<N\text{-}1>} & \ldots & U_{1(N\text{-}1)<N\text{-}1>} & U_{1N<N\text{-}1>} \end{bmatrix}^{-1} \times \begin{bmatrix} q_{1<1>} \\ q_{1<2>} \\ \vdots \\ q_{1<N\text{-}2>} \\ q_{1<N\text{-}1>} \end{bmatrix} \tag{18}$$

where $q_{1<k>}$ is the charge distributions of the first turn, $U_{12<k>} \ldots U_{1N<k>}$ ($k = 1,2 \ldots N$-1) are the voltage between the first turn and other turns when the matrix of charge distributions of winding is $[q]_{<k>}$.

Based on the above model, the energy in the edge can be calculated and added to the W_{ll}.

The above steps can be summarized as a flowchart shown in Fig.11.

IV. THE ANALYSIS OF SIMULATION AND EXPERIMENT

A high-frequency inductor is adopted to verify the correctness of the theoretical analysis. Its 3D FEA simulation model is shown in Fig. 11. The calculated and simulation results of C_D at different r_0 are shown in Fig. 12.

Fig. 12(a) compares the traditional capacitance calculation method with the proposed method under different wire diameters. Fig. 12(b) shows the error of the two methods. With the proposed method, the capacitance value has a smaller error over the different wire diameter gauges. Furthermore, the larger the wire diameter, the smaller the error, and the error is reduced by 12% at a wire diameter of 0.95mm.

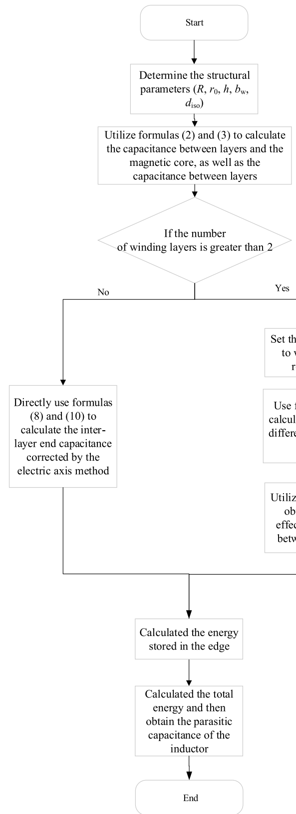

FIGURE 11. The simulation model of high frequency inductor.

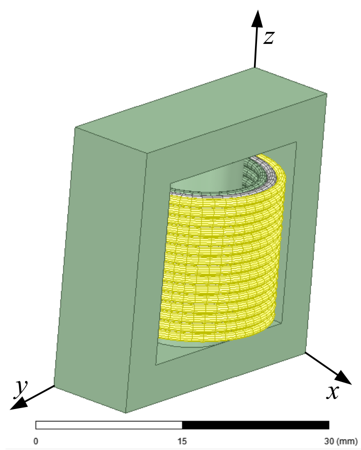

FIGURE 12. The simulation model of high-frequency inductor.

According to Fig. 13, the C_D values of simulation and calculation are almost consistent. Moreover, the maximum error is less than 8%. Finally, an inductor is made to verify the correctness of the calculation model. And the parameters of inductor are as follow: h = 1.057mm, d_w = 15.698mm, r_0 =0.9mm, d_{iso} = 0.1mm, d_{core1} = 1.595mm, d_{core2} = 1.175mm, $R(i)$ = 6.925mm, $R_1(i)$ = 4.88mm and $R_2(i)$ = 9.375mm. The core material is PC40, and the relative permittivity of the insulating layer is 4.4. The distributed capacitance C_D of the inductor is measured by impedance analyzer WK6500B in Fig. 13, and the comparison between simulated, measured and calculated values of C_D is in Table 1. The impedance characteristic curve is shown in Fig.14, and since this article focuses only on the value of the capacitor, the inductance value is fitted using the actual value. It can be observed that the measured and calculated values are almost the same.

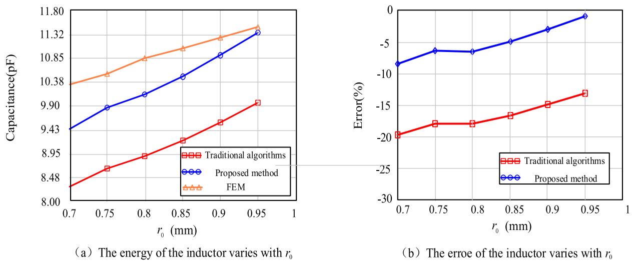

FIGURE 13. **The calculated and simulation values of C_D at different wire gauges.**

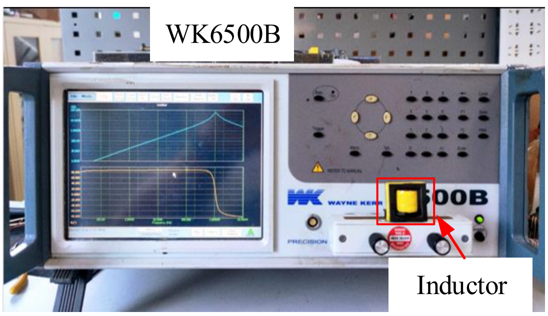

FIGURE 14. **Experimental platform.**

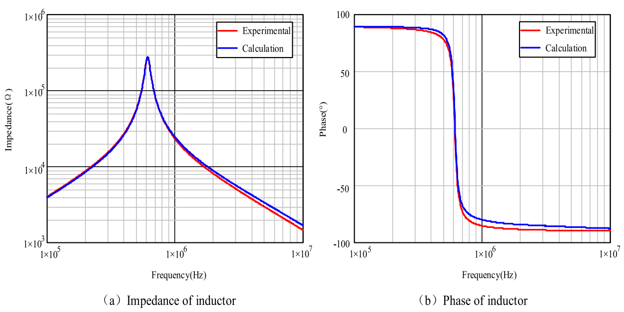

FIGURE 15. **Inductor's frequency response.**

According to Table 1, the simulation and measured value of distributed capacitance C_D are almost the same, and the error of calculated and measured is 0.46%. FEM and experiments verify the accuracy of the edge effect calculation method in the multilayer winding structure.

TABLE 1. **The Comparison of C_D.**

Parameters	Calculation Value	Simulation value	Measured value
C_D (pF)	10.91	11.2	10.86

V. CONCLUSION

This study analyzes the parasitic capacitance of high-frequency magnetic components. Furthermore, a calculation model of parasitic capacitance is proposed. The conclusions are summarized as follows:

(a) The analysis explores the sources and effects of edge effects, indicating that when the d/h is relatively large, the impact of end effects becomes significant and cannot be ignored.

(b) A new method to calculate the edge effect capacitance of the inductor is proposed. This method can accurately calculate the non-adjacent turn capacitance.

(c) Finally, the parasitic capacitance of the inductor is obtained by the energy method. The simulation and measured results verify the feasibility of the proposed calculation model.

REFERENCES

[1] C. Gu, Z. Zheng, L. Xu, K. Wang, and Y. Li, "Modeling and control of a multiport power electronic transformer (PET) for electric traction applications," *IEEE Trans. Power Electron.*, vol. 31, no. 2, pp. 915–927, Feb. 2016.

[2] R. Wang, F. Xiao, Z. Zhao, Y. Shen, and G. Yang, "Effects of asymmetric coupling on winding AC resistance in medium-frequency high-power transformer," *IEEE Trans. Magn.*, vol. 50, no. 11, pp. 1–4, Nov. 2014.

[3] N. T. Tran, T. P. Nguyen, D. L. Ho, T. M. T. Pham, and D. A. K. Pham, "Capacitances in a physical distributed circuit of a black-box power transformer for frequency response analysis at medium frequencies," in *Proc. IEEE Int. Conf. High Voltage Eng. Appl. (ICHVE)*, Chengdu, China, Sep. 2016, pp. 1–4.

[4] S. Jeong, D. Shin, and J. Kim, "A transformer-isolated common-mode active EMI filter without additional components on power lines," *IEEE Trans. Power Electron.*, vol. 34, no. 3, pp. 2244–2257, Mar. 2019, doi: 10.1109/TPEL.2018.2845467.

[5] K. Zhang, W. Chen, X. Cao, P. Pan, S. W. Azeem, G. Qiao, and F. Deng, "Accurate calculation and sensitivity analysis of leakage inductance of high-frequency transformer with Litz wire winding," *IEEE Trans. Power Electron.*, vol. 35, no. 4, pp. 3951–3962, Apr. 2020.

[6] N. B. Chagas and T. B. Marchesan, "Analytical calculation of static capacitance for high-frequency inductors and transformers," *IEEE Trans. Power Electron.*, vol. 34, no. 2, pp. 1672–1682, Feb. 2019.

[7] M. S. Sanjari Nia, P. Shamsi, and M. Ferdowsi, "Investigation of various transformer topologies for HF isolation applications," *IEEE Trans. Plasma Sci.*, vol. 48, no. 2, pp. 512–521, Feb. 2020.

[8] M. Popov, R. Smeets, L. van der Sluis, H. de Herdt, and J. Declercq, "Experimental and theoretical analysis of vacuum circuit breaker prestrike effect on a transformer," *IEEE Trans. Power Del.*, vol. 24, no. 3, pp. 1266–1274, Jul. 2009.

[9] Z. De Grève, O. Deblecker, and J. Lobry, "Numerical modeling of capacitive effects in HF multiwinding transformers—Part II: Identification using the finite-element method," *IEEE Trans. Magn.*, vol. 49, no. 5, pp. 2021–2024, May 2013.

[10] C. Liu, L. Qi, X. Cui, and X. Wei, "Experimental extraction of parasitic capacitances for high-frequency transformers," *IEEE Trans. Power Electron.*, vol. 32, no. 6, pp. 4157–4167, Jun. 2017.

[11] X. Liu, Y. Wang, J. Zhu, Y. Guo, G. Lei, and C. Liu, "Calculation of capacitance in high-frequency transformer windings," *IEEE Trans. Magn.*, vol. 52, no. 7, pp. 1–4, Jul. 2016.

[12] X. Wei, Z. Zhengming, and J. Qirong, ''Calculation method of distributed capacitance of high frequency transformer,'' *J. Tsinghua Univ., Sci. Technol.*, vol. 61, no. 10, pp. 1088–1096, Jul. 2021.
[13] L. Dalessandro, F. D. S. Cavalcante, and J. W. Kolar, ''Self-capacitance of high-voltage transformers,'' *IEEE Trans. Power Electron.*, vol. 22, no. 5, pp. 2081–2092, Sep. 2007.
[14] P. Thummala, H. Schneider, Z. Zhang, and M. A. E. Andersen, ''Investigation of transformer winding architectures for high-voltage (2.5 kV) capacitor charging and discharging applications,'' *IEEE Trans. Power Electron.*, vol. 31, no. 8, pp. 5786–5796, Aug. 2016.
[15] Z. Shen, H. Wang, Y. Shen, Z. Qin, and F. Blaabjerg, ''An improved stray capacitance model for inductors,'' *IEEE Trans. Power Electron.*, vol. 34, no. 11, pp. 11153–11170, Nov. 2019.
[16] Z. Shen and H. Wang, ''Parasitics of orthocyclic windings in inductors and transformers,'' *IEEE Trans. Power Electron.*, vol. 36, no. 2, pp. 1994–2008, Feb. 2021.
[17] L. Deng, P. Wang, X. Li, H. Xiao, and T. Peng, ''Investigation on the parasitic capacitance of high frequency and high voltage transformers of multi-section windings,'' *IEEE Access*, vol. 8, pp. 14065–14073, 2020.
[18] D. Ahmed, L. Wang, M. Wu, L. Mao, and X. Wang, ''Two-dimensional winding loss analytical model for high-frequency multilayer air-core planar inductor,'' *IEEE Trans. Ind. Electron.*, vol. 69, no. 7, pp. 6794–6804, Jul. 2022, doi: 10.1109/TIE.2021.3102451.
[19] F. Robert, P. Mathys, B. Velaerts, and J.-P. Schauwers, ''Two-dimensional analysis of the edge effect field and losses in high-frequency transformer foils,'' *IEEE Trans. Magn.*, vol. 41, no. 8, pp. 2377–2383, Aug. 2005, doi: 10.1109/TMAG.2005.852938.
[20] X. Wang, L. Wang, L. Mao, and Y. Zhang, ''Improved analytical calculation of high frequency winding losses in planar inductors,'' in *Proc. IEEE Energy Convers. Congr. Expo. (ECCE)*, Portland, OR, USA, Sep. 2018, pp. 4336–4340, doi: 10.1109/ECCE.2018.8558397.

YUJIE LAN was born in Fujian, China, in 1998. He received the B.S. degree in electrical engineering and automation from the Harbin University of Science and Technology, Guangzhou, China, in 2021. He is currently pursuing the master's degree with Fuzhou University, Fuzhou. His research interest includes high frequency magnetic technology.

LEI YANG was born in Henan, China, in 1982. He received the Ph.D. degree in aerospace propulsion from the Beijing Institute of Technology, Beijing, China, in 2014. He is currently a Senior Engineer with the Beijing Institute of Precision Mechatronics and Controls. His research interest includes aerospace servo power technology.

XU ZHANG was born in Fuzhou, China, in 1998. He received the B.S. degree in electrical engineering and automation from Northeast Agricultural University, Harbin, China, in 2016, and the master's degree in electrical engineering and automation from Fuzhou University, Fuzhou, in 2023. His research interest includes high frequency magnetic technology.

QINGBIN CHEN was born in Quanzhou, China. He received the B.E. and Ph.D. degrees in electrical engineering from Fuzhou University, Fuzhou, China, in 2007 and 2012, respectively. He was a Visiting Scholar with the University of Florida, Gainesville, FL, USA, from 2017 to 2018. His research interests include high frequency magnetic technology, EMC diagnosis and suppression technology, and wireless power transfer. He is a member of the Magnetic Components and Ferrite Materials (Magnetic Standards Committee of China). He served as the Vice Chairperson and the Deputy Secretary General for the Magnetic Component Specialty Committee of the China Power Supply Society (CPSS).

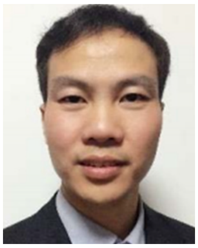

ZAIPING ZHENG was born in Zhejiang, China, in 1979. He received the B.Sc. degree in automation from Harbin Engineering University, Harbin, China, in 2002, and the M.Sc. degree in control engineering from the Beijing University of Aeronautics and Astronautics, Beijing, China, in 2012. He is currently employed at the Beijing Institute of Precision Mechatronics and Controls. His current research interests include control methods applied to multiphase fault tolerant permanent magnet synchronous machines and PMSM systems.